Biophysical Journal Volume 70 January 1996 38–47

Spectral Analysis of Muscle Fiber Images As a Means of Assessing Sarcomere Heterogeneity

M. P. Slawnych, L. Morishita, and B. H. Bressler
Department of Anatomy, University of British Columbia, Vancouver, British Columbia, Canada.

ABSTRACT A new image-analysis-based method is described for assessing sarcomere heterogeneity in skinned rabbit psoas muscle fiber segments. This method consists of off-line, two-dimensional Fourier spectral analysis of video-taped muscle images. Local sarcomere length is assessed by partitioning the muscle images into half and quarter images spanning the original image and analyzing the associated spectra. The spectra are analyzed in two different ways, yielding two measures of sarcomere length. The first measure is obtained by calculating and inverting the centroid frequency of the first-order peak associated with each two-dimensional Fourier spectrum. The second measure is obtained in a similar manner, the only difference being that the two-dimensional spectra are first collapsed into one-dimensional line spectra by summing the pixels perpendicular to the fiber axis. Comparison of the two measures provides a measure of striation skewness that cannot be obtained by other image analysis based methods that determine sarcomere length by analyzing selected line luminance profiles.

INTRODUCTION

Sarcomere length quantification is central to studies examining the mechanical properties of single muscle fibers and is generally performed by using methods based around laser diffraction (cf. Lieber et al., 1984). By capitalizing on the natural optical phase grating provided by the regular arrangement of the thick and thin filaments, these methods offer high spatial and temporal resolution of sarcomere length. In addition, they can readily be adapted to sarcomere length clamping (Goldman and Simmons, 1979). However, in the vast majority of methods in which it is implemented, laser diffraction provides only a measurement of the average periodicity of the sarcomeres illuminated by the laser and hence is not well suited to the analysis of local sarcomere dynamics. It should be noted that a significant effort has been directed toward understanding the fine details of the diffraction spectra and relating these details to the underlying sarcomeric organization (Rudel and Zite-Ferenczy, 1979; Yeh et al., 1980; Judy et al., 1982; Leung, 1982, 1984; Brenner, 1985; Sundell et al., 1986; Zite-Ferenczy et al., 1986; Roos and Leung, 1987; Thornhill et al., 1991; Sidick et al., 1994). For example, using numerical methods, Judy and colleagues were able to show that the fine meridonal features lying within the diffractin peaks could be interpreted in the context of discrete sarcomere populations. However, this level of analysis is not generally used to examine the dynamics of local sarcomere behavior. Local sarcomere dynamics can play a significant role in influencing the observed contractile response (Huxley and Peachey, 1961; Julian et al., 1978). As a result, a number of investigators have turned to image analysis as a means of examining local sarcomere behavior. A number of such methods have been proposed, ranging from relatively fast, single-line charge coupled device–based methods to slower video analysis and off-line cine-film-based methods (Goldspink et al., 1970; Kawai and Kuntz, 1973; Krueger et al., 1980; Roos and Brady, 1982; Roos et al., 1982; Lieber et al., 1983; deClerck et al., 1984; Roos, 1987; Krueger, 1988; Roos and Taylor, 1988; Roos et al., 1989; Periasamy et al., 1990; Krueger and Denton, 1991; Anazawa et al., 1992; Horowitz et al., 1992; Gannier et al., 1993). In the majority of these methods, sarcomere length assessment is carried out directly in the spatial domain. Analysis methods vary from the manual assessment of cine or video images to the more quantitative assessment of the peaks and nadirs of luminance lines intersecting the muscle fiber segments (Roos and Brady, 1982; Roos et al., 1982; Horowitz et al., 1992; Roos and Taylor, 1993). To characterize the sarcomere length distribution of the fiber across its entire width, multiple luminance profiles spanning the fiber width have to be acquired and analyzed. However, such analysis is sensitive to local image quality. This is highlighted in Fig. 1, which shows some luminance profiles obtained from selected regions of an individual muscle fiber segment. The middle and bottom luminance profiles represent the ideal situation in which there is little amplitude variation between successive peaks and nadirs. The top luminance profile, on the other hand, shows an example in which there can be a large amount of interpeak and internadir variation. This variation, which is at least partly due to the presence of nonstriated material, complicates the process of detecting successive peaks and nadirs. Specifically, a few of the peaks are significantly smaller than the remaining peaks and, without any additional signal processing, could easily be missed by threshold-based peak detection methods. Although signal-processing measures such as bandpass filtering can be readily implemented, there may be instances in which the

Received for publication 20 March 1995 and in final form 4 October 1995.

Address reprint requests to Dr. Michael P. Slawnych, Department of Anatomy, University of British Columbia, 2177 Wesbrook Mall, Vancouver, B.C. V6T 1Z3, Canada. Tel.: 604-822-2680; Fax: 604-822-2316; E-mail: slawnych@unixg.ubc.ca.

0006-3495/96/01/38/10 $2.00

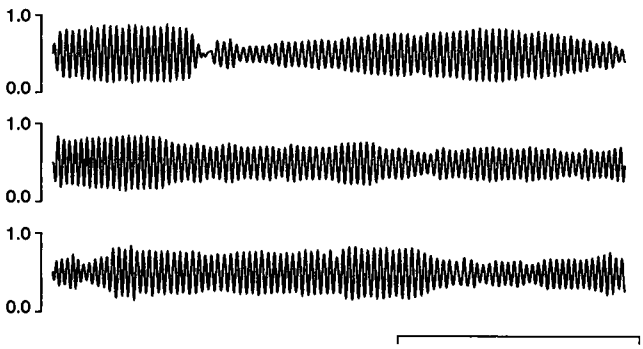

FIGURE 1 Line luminance profiles obtained from top, middle, and bottom regions of the fiber segment shown in Fig. 4 *a* below. The peaks and nadirs correspond to the I and A bands of the striation pattern, respectively. The labels on the ordinate axes indicate relative luminance. The calibration line represents 100 μm.

peaks of the processed signal are still below threshold levels and hence not identified. Fourier analysis, on the other hand, is not so adversely affected by such variation. Specifically, muscle fibers can be considered periodic patterns, and, as such, the line luminance profiles can be represented in terms of Fourier spectra. Fourier analysis can also be used to study the full two-dimensional image of the muscle fiber, which has important implications in terms of being able to examine striation skewness. Ideally, when the striations are normal to the long axis of the fiber, the first- (and higher-) order spectral density peaks are located on the long, or equatorial, axis of the Fourier spectrum (Fig. 2 *b*). In this situation, both one- and two-dimensional-based Fourier analysis will yield identical results. Skewness results in the appearance of nonequatorial components (Fig. 2 *d*) that would not be detected by one-dimensional-based analysis (i.e., analysis of individual luminance patterns). Ignoring the nonequatorial frequency component introduces an error in the sarcomere length measurement, the magnitude of which varies with the severity of striation skewness (Fig. 3). It should be noted that in the majority of the sarcomere length detection methods based around laser diffraction the two-dimensional diffraction pattern is compressed into a one-dimensional line spectrum, which is then acquired by using a linear (i.e., one-dimensional) photodiode array. Although this yields better temporal resolution than would be achievable by acquiring the two-dimensional diffraction pattern, the resultant line spectrum is insensitive to striation skewness.

We present a new image-analysis-based method that addresses the above issues. It is based on the calculation and examination of two-dimensional Fourier power spectra of muscle images. This transformation can be carried out efficiently by using the fast Fourier transform (Cooley and Tukey, 1965). The magnitude of the transformed image represents the spectral energy density in the frequency domain. Assuming that the centroid frequency of the first-order spectral density peak represents

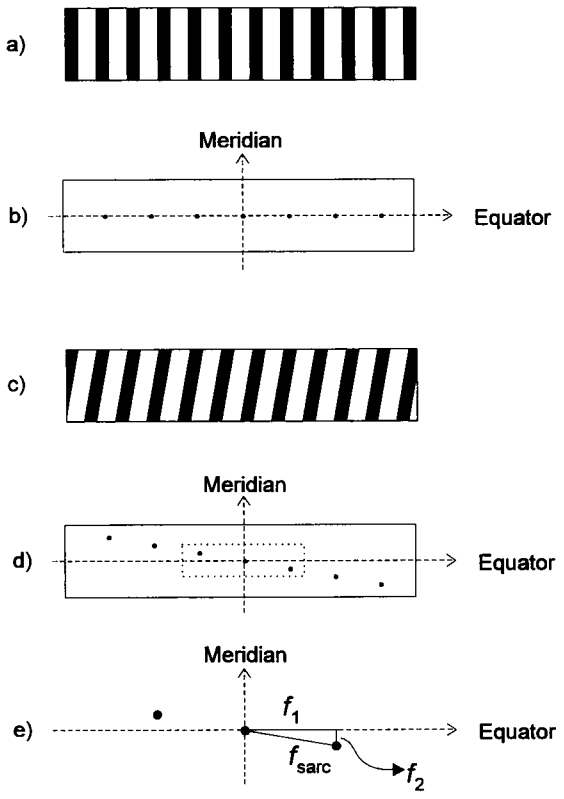

FIGURE 2 (*a*) Example of a muscle image in which the striations are normal to the fiber axis. (*b*) Associated Fourier spectra, showing the first- and higher-order spectral peaks falling on the fiber axis. (*c*) Sample muscle image in which the striations are skewed relative to the fiber axis. (*d*) Associated Fourier spectra, showing the first- and higher-order spectral peaks located off of the fiber axis. (*e*) Enlargement of the dotted area in (*d*), showing the equatorial and meridinal components of the first-order diffraction peak. By definition, we have that $f_{sarc} = ((f_1)^2 + (f_2)^2)^{1/2}$. When no striation skewness is present, $f_2 = 0$, and hence $f_{sarc} = f_1$.

the fundamental sarcomeric frequency, the mean sarcomere length is simply given by the reciprocal of this frequency. We evaluate the spectrum associated with the full muscle image. In addition, the image is partitioned into several subimages spanning the original image; by evaluating the associated Fourier spectra, local sarcomere heterogeneity and skewness are assessed.

MATERIALS AND METHODS

Preparations

Psoas muscles were obtained from adult rabbits and chemically skinned according to the standard protocol (Moss et al., 1983). Single fiber segments, typically shorter than 500 μm, were isolated and mounted horizontally between a force transducer (SensoNor, Horten, Norway; Model AE801) and a servomotor (Cambridge Technologies, Cambridge, MA; Model 300S), using aluminum foil T-clips, and then submerged in a chamber containing relaxing solution (pCa 9.0). The force transducer had a resonant frequency of ~2.5 kHz in air. Care was taken in mounting the fiber segments to ensure that they were not twisted. The chamber volume was ~200 μl. The chamber walls were made of Plexiglas and contained cooling channels to facilitate temperature control. Experiments were carried out at 10 ± 1°C. The chamber bottom was made of glass, permitting

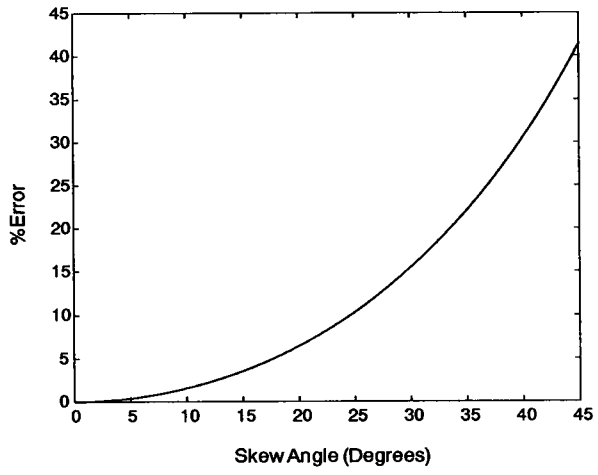

FIGURE 3 Error in sarcomere length introduced by ignoring the nonequatorial component of the spectral diffraction peak as a function of skew angle. By definition, this error is defined as $sl_{err} = (1/f_1 - 1/f_{sarc})/(1/f_{sarc})$, where f_{sarc} is the frequency of the first-order spectral peak as measured in the two-dimensional frequency space and f_1 is the equatorial component. For a skew angle of θ, this reduces to $sl_{err} = 1/\cos(\theta) - 1$.

the fiber to be visualized along the vertical axis. The experimental chamber and associated apparatus were placed on the stage of an inverted microscope (Nikon; Diaphot 300). The microscope was mounted on an air-suspension table system. Fiber segments were illuminated by a halogen light source filtered to 546 nm using a green interference, which represents the best compromise between microscope resolution and CCD sensitivity (Inoue, 1986). The segments were visualized using 40× (N.A. = 0.55, depth of field ≈ 4 μm) and 20× (N.A. = 0.40, depth of field ≈ 6 μm) objectives in conjunction with a 10× ocular, yielding total magnifications of 400× and 200×, respectively. The condenser aperture was set at its full open setting. A charge coupled device video camera (Cohu, San Diego, CA; Model 4910) was connected to the video port of the microscope, which in turn was connected to both a video monitor and an S-VHS video recorder.

Solutions

All solutions were 200-mM total ionic strength and contained 93-mM potassium, 40-mM sodium, 5-mM MgATP, 1-mM free magnesium, 15-mM creatine phosphate, and 0.1-mg/ml creatine phosphokinase. The solution pH was 7.0 in a MOPs buffer. Propionate was the major anion. Calcium concentration was controlled by an EGTA buffer system (15 mM). All solutions contained 0.5-mM Dithiothreitol to prevent protein degradation. Dextran T-70 (11.2%) was also added to all solutions to restore the fiber diameters to preskinning levels (Ford et al., 1991).

Experimental protocol

First the fiber segment was set to the desired mean sarcomere length. A contraction was then initiated by transferring the fiber into a high-concentration calcium solution (pCa 4.5). After maximum tension was reached, the contraction was terminated by transferring the fiber back into the relaxing solution. All contractions were video taped for subsequent image analysis.

Measurements

The raw signal produced by the force transducer was first amplified and then fed to a digital oscilloscope (Tektronix, Beaverton, OR; Model TDS 420). It was converted to force units using a calibration factor obtained with a set of standard weights. The sarcomere length was assessed by off-line analysis of video images of the fiber, which were digitized at a resolution of 640× 480 with a frame-grabber board (Imaging Technologies, Woburn, MA; Model OFG640) that contained an 8-bit flash analog-to-digital converter operating at 12.5 MHz. The video analysis system was calibrated with a precision grating (Graticules Ltd., Tonbridge, England).

Sarcomere length for all fiber segments was calculated by evaluating the Fourier spectra for both the full image and separate subimages spanning the fiber. Specifically, muscle images were partitioned into two half-images and four quarter images, which were used to assess local sarcomere heterogeneity. All images were multiplied by a two-dimensional Hanning window before calculation of the spectra. Sarcomere length was calculated by taking the inverse of the centroid frequency of the first-order peak. In addition, the two-dimensional image spectra were also compressed into one-dimensional line spectra by summing the pixels perpendicular to the fiber axis, which is functionally equivalent to using a cylindrical lens to obtain line spectra from fibers subjected to laser diffraction. Again, we calculated and inverted the centroid frequencies of the first-order peaks to arrive at the sarcomere lengths. As stated earlier, the latter measure of sarcomere length eliminates the nonequatorial frequency component of the first-order peak (which indicates striation skewness) from the sarcomere length calculation.

RESULTS

Fig. 4 *a* shows an image of a fiber segment and its associated full, half, and quarter spectra immediately before immersion in the activating solution. It can be readily seen that the striations are well ordered and normal to the fiber axis. This is confirmed by the image spectra, which contain distinct first-order diffraction peaks situated on the fiber axis. To facilitate the comparison of these spectra, the associated line spectra are plotted in Fig. 5 *a*, where we see good correspondence between the individual spectra (in terms of localization of the first order spectral peaks). The associated sarcomere length measures are listed in Table 1. As we can readily see, there is good agreement between the sarcomere lengths derived from the two-dimensional image spectra and their associated one-dimensional line spectra.

Fig. 4 *b* shows the same fiber segment (and its associated spectra) during activation. In this case, the striations are not so well ordered, which results in some meridional streaming of the first- and higher-order diffraction peaks in the associated spectra. The associated line spectra are plotted in Fig. 5 *b*. Although there is good correspondence in terms of peak localization, the peak widths have increased, which is indicative of increased disorder (Table 2). In addition, the standard deviations of the half- and quarter-image-based sarcomere length measures (normalized by their respective means) have increased, as shown in Table 1. However, this increased disorder is not associated with any large scale change in striation skewness, as confirmed by the relatively small differences between the two different sarcomere length measures.

In Fig. 6 we compare the sarcomere length signals derived from the full and partial images as a function of time before, during, and after activation. The sarcomere behavior derived from the full image indicates a small amount of shortening during activation. Analysis of the two half-

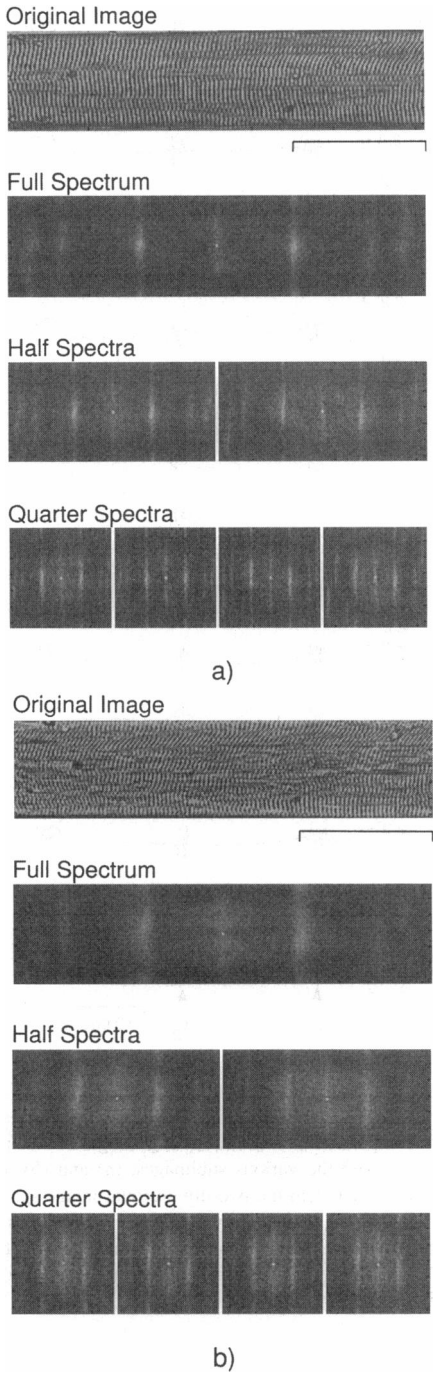

FIGURE 4 Comparison of Fourier spectra (*a*) before and (*b*) during muscle contraction. In each case, the top figure represents the original fiber image, the second represents the power spectrum associated with the entire fiber image, the third represents the power spectra associated with the left and right half-images, and the fourth represents the power spectra associated with the quarter images. The calibration line represents 100 μm.

images (H1 and H1), on the other hand, shows that the sarcomeres in the left half of the image undergo some shortening during activation, whereas the right half sarcomeres do not. Analysis of the quarter images also show shortening in the far left and middle left quarters (Q1 and Q2, respectively), whereas analysis of the far right quarter

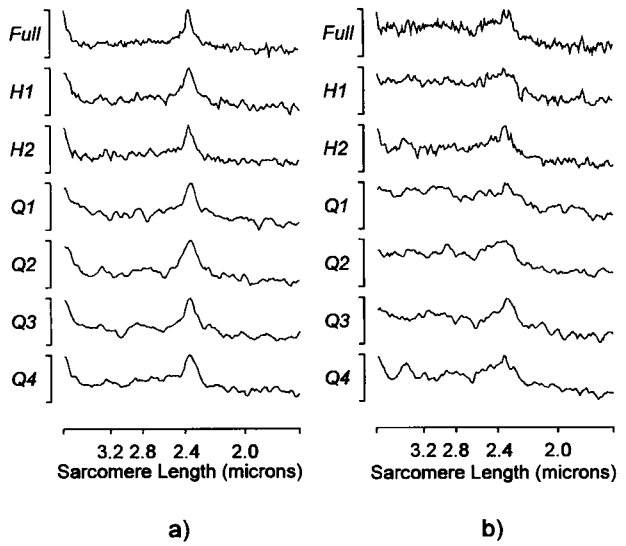

FIGURE 5 Line spectra corresponding to the spectral images in Fig. 4. The abscissa indicates frequency, ranging from dc to $f_s/2$ (some corresponding sarcomere lengths are indicated in micrometers). The ordinate axes indicate relative amplitude on a logarithmic scale.

image (Q4) indicates lengthening. Hence, the sarcomere length derived form the full image is not indicative of the local sarcomere behavior.

In general, we found that the fiber segments initially exhibited little skewness, and hence the sarcomere lengths derived from the two-dimensional spectra were very similar to those derived from the one-dimensional line spectra. An example of this can be found in Table 1, where there is little difference between the two sarcomere length measures, even during contraction. However, as the fiber segments underwent an increased number of contraction cycles, the degree of skewness usually increased in the majority of the fibers that we examined. In addition, increased skewness also tended to be associated with longer sarcomere lengths.

TABLE 1 Comparison of sarcomere lengths derived from the two-dimensional image spectra and associated one-dimensional line spectra

Image Segment	Image a		Image b	
	SL_{2D}	SL_{1D}	SL_{2D}	SL_{1D}
Full	2.41	2.41	2.27	2.28
H1	2.40	2.40	2.29	2.29
H2	2.41	2.41	2.37	2.37
Q1	2.38	2.38	2.30	2.30
Q2	2.38	2.38	2.37	2.37
Q3	2.39	2.39	2.30	2.30
Q4	2.41	2.41	2.38	2.38
ΔH^*	0.10	0.12	2.17	2.17
$\Delta Q^\ddagger$	0.48	0.50	1.84	1.84

*ΔH is the standard deviation of the half-image sarcomere length measures normalized by the mean sarcomere length obtained from the half-images.
‡ΔQ is the standard deviation of the quarter image sarcomere length measures normalized by the mean sarcomere length obtained from the quarter images.

TABLE 2 Comparison of the widths of the spectral peaks illustrated in Fig. 4 *a* and *b

Image Segment	Peak Width (μm) for Image a	Peak Width (μm) for Image b
Full	0.08	0.20
H1	0.13	0.39
H2	0.09	0.15
Q1	0.18	0.38
Q2	0.23	0.76
Q3	0.16	0.27
Q4	0.21	0.29

*Peak widths were calculated by evaluating the differences between the sarcomere lengths associated with the spectral peak frequencies at which the amplitudes of the spectral peak dropped to $1 - e^{-1}$ ($\cong$63%) of the maximum value.

An example of this is shown in Fig. 7, where the images obtained from the same fiber segment at two different sarcomere lengths are compared. It can readily be observed that the spectral peaks associated with the image in which the striations are skewed are located off the equatorial axis. As a consequence, there is a difference between the sarcomere lengths derived from the two-dimensional image spectra and the associated line spectra (the latter are plotted in Fig. 8). These sarcomere lengths are listed in Table 3. Looking at this table, we see that the differences as large as 0.41 μm are observed. In addition, there is increased disorder in the image associated with the longer sarcomere lengths, which can be viewed both in terms of the increased values of the normalized standard deviations of the half- and quarter-image-based sarcomere length measures (Table 3) and increased widths of the first-order diffraction peaks in Fig. 8. The widths of these peaks are tabulated in Table 4.

The muscle fiber segment illustrated in the right half of Fig. 7 represents an interesting case inasmuch as there is a progressive increase in striation skewness as we move from left to right. Whereas the sarcomere length measures listed in Table 3 indeed indicate that skewness is increasing, a more comprehensive assessment can be obtained by partitioning the image into even smaller subimages. The results of such an analysis are shown in Fig. 9, where we see a progressive increase in the difference between the two different sarcomere length measures as we move along the fiber axis. In terms of the source of the skewness, it may represent the "failure" of specific sarcomeres in individual myofibrils distributed throughout the fiber segment (Morgan 1990a, b). Alternatively, it may also represent the torsional response of the fiber in situations in which the fiber is twisted with respect to its natural orientation. As stated, care was taken to minimize such twisting during mounting.

In addition to the centroid frequencies of the diffraction peaks, the frequencies at which the diffraction peaks reached their maximum values were also calculated, and these were inverted to yield an alternative sarcomere length measure. Niggli (1988) has stated that the latter measure is less sensitive to the signal-to-noise ratio of the diffraction

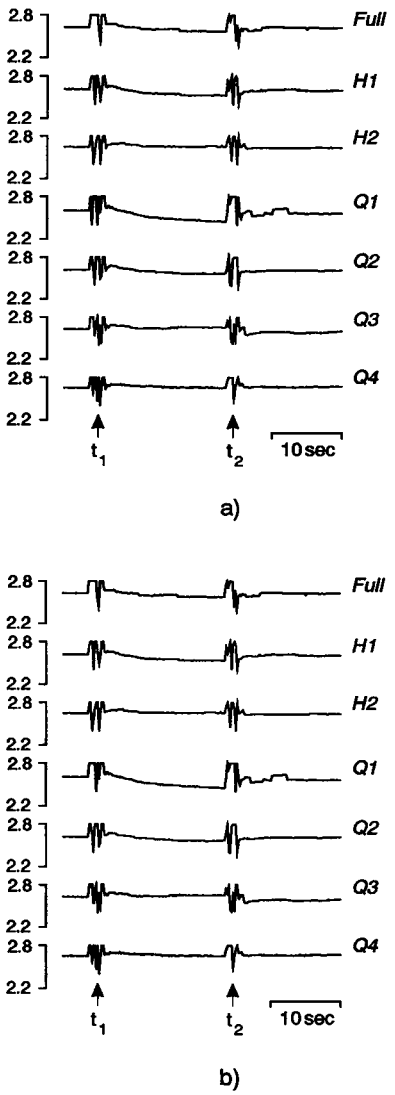

FIGURE 6 Comparison of sarcomere length signals obtained from the full muscle image and the various subimages. (*a*) and (*b*) represent sarcomere lengths derived from the two-dimensional image spectra and one-dimensional line spectra, respectively. The fiber was transferred from the relaxing solution to the activation solution during t_1 and returned to the relaxing solution during t_2. The labels on the ordinate axes indicate sarcomere length in micrometers.

spectra than the centroid-based measure and has used it to examine sarcomere dynamics in isolated cardiac myocytes. We found that there was only a minimal difference between the two different sarcomere length measures.

DISCUSSION

As we have stated, sarcomere length heterogeneity plays a central role in studies involving muscle mechanics. Although sarcomere length is generally assessed by techniques based around laser diffraction, it has been suggested that laser diffraction is not an appropriate method to examine sarcomere heterogeneity because it detects only those striations that are regular over a large number of sarcomeres

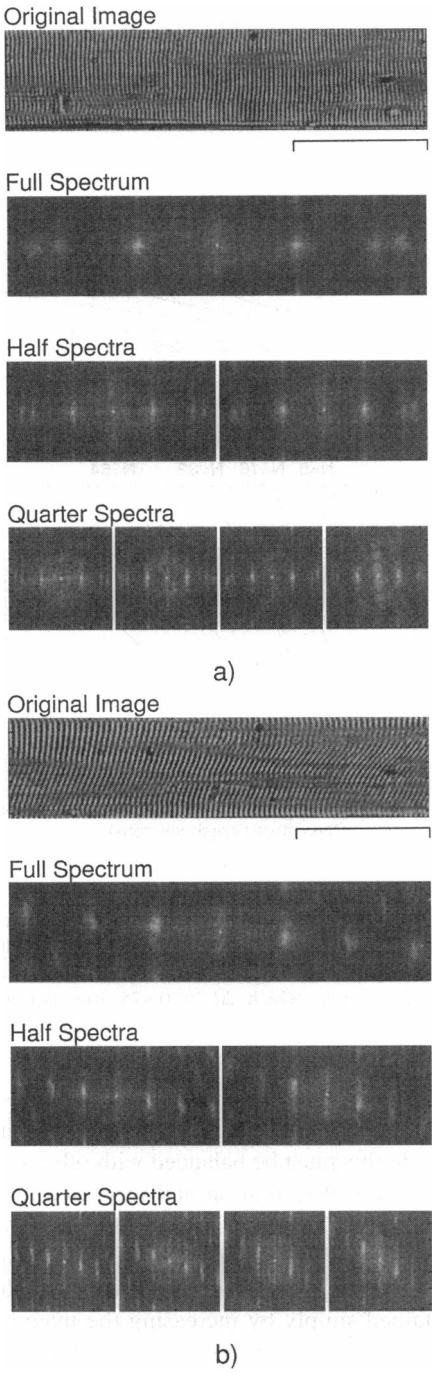

FIGURE 7 Comparison of images and associated spectra of a fiber segment stretched to two different sarcomere lengths. Again, the top figures represent the original fiber images, the second images represent the power spectra associated with the entire fiber images, the third represent the power spectra associated with the left and right half-images, and the fourth represent the power spectra associated with the quarter images. The calibration line represents 100 μm.

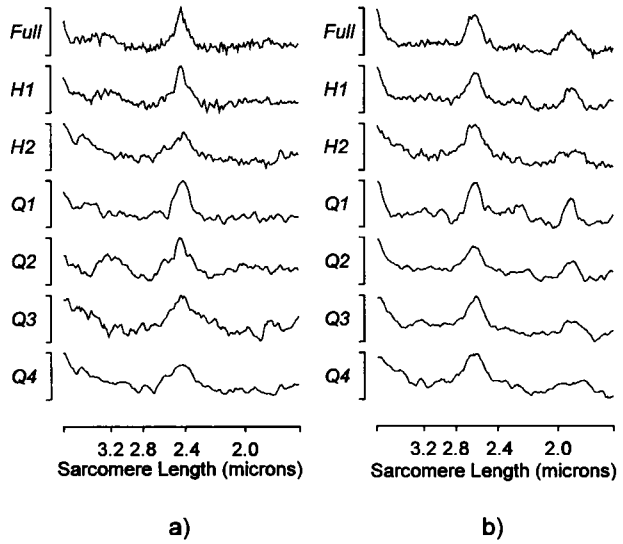

FIGURE 8 Line spectra corresponding to the spectral images in Fig. 7. The abscissa indicates frequency, ranging from dc to $f_s/2$, and the ordinate axes indicate relative amplitude on a logarithmic scale.

and thus may miss small populations of nonuniform sarcomeres (Huxley, 1980). In addition, when the striations are not normal to the image plane, Bragg artifacts can cause erroneous sarcomere-length readings (Rudel and Zite-Ferenczy, 1979; Goldman and Simmons, 1984). Finally, as the diffraction images are usually compressed and focused onto one-dimensional photosensor arrays, information relating to fiber skewness is lost. Image-analysis-based methods, on the other hand, are well suited to examining local sarcomere dynamics. The main disadvantage of using image analysis to assess sarcomere heterogeneity is that it does not offer the same spatial and temporal resolution as that obtained by laser-diffraction-based methods. Spatial resolution is governed by two factors: the resolving power of the microscope and the resolution with which the image is digitized. For the magnifications and optics used here, spatial resolution is determined mainly by the latter. Specifically, according to the Rayleigh criterion, the minimum resolution is 0.627 and 0.862 μm when the 40× and 20× objectives are employed, respectively. However, it should be noted that the Rayleigh criterion provides only an approximate estimate of the actual resolution (cf. Roos and Brady, 1982; Gannier et al., 1993). In terms of digitization effects, to simplify matters, let us assume that the frequency

TABLE 3 Comparison of sarcomere lengths derived from the two-dimensional image spectra and associated one-dimensional line spectra

Image Segment	Image a		Image b	
	SL_{2D}	SL_{1D}	SL_{2D}	SL_{1D}
Full	2.52	2.52	2.81	3.09
H1	2.51	2.51	2.82	3.08
H2	2.48	2.48	2.77	3.11
Q1	2.49	2.49	2.8	3.09
Q2	2.49	2.49	2.8	3.09
Q3	2.49	2.49	2.76	3.11
Q4	2.49	2.49	2.74	3.15
ΔH	0.85	0.85	1.26	0.69
ΔQ	0.00	0.00	1.08	0.91

TABLE 4 Comparison of the widths of the spectral peaks illustrated in Fig. 4 *a* and *b*

Image Segment	Peak Width (μm) for Image a	Peak Width (μm) for Image b
Full	0.08	0.25
H1	0.14	0.24
H2	0.12	0.42
Q1	0.20	0.30
Q2	0.19	0.36
Q3	0.19	0.45
Q4	0.28	0.53

of spectral density point associated with the maximal amplitude, as opposed to the centroid frequency, is used to obtain the sarcomere length. Under these conditions the frequency of the maximum amplitude point can assume one of $N/2 + 1$ levels uniformly distributed between 0 and $f_s/2$, where N is the number of pixels used to represent the image in the axial direction and f_s is the sampling frequency. The latter is simply given by the reciprocal of the resolution with which the image is digitized in the spatial domain (i.e., $1/\Delta l$). Although the frequency values are uniformly distributed on the frequency axis, the reciprocals of these frequencies, which yield the sarcomere lengths, are not uniformly distributed. In particular, as the frequency increases (and hence the sarcomere length decreases), the differences between successive sarcomere length levels decrease. Therefore, the sarcomere length resolution will depend on three factors: Δl, N, and the actual sarcomere length. Fig. 10 *a* shows the relation between sarcomere length resolution and sarcomere length for three different values of Δl (0.2375, 0.475, and 0.950 μm, corresponding to magnifications of 400×, 200×, and 100×, respectively) for the case in which $N = 512$. For any given value of Δl, the sarcomere length resolution decreases as the sarcomere length decreases. For example, at a sarcomere length of 2.5 μm the resolution at 400× magnification is of the order of 0.1 μm and would result in a "choppy"-looking sarcomere length signal. Although better resolution can be obtained by using lower magnification, this must be balanced with other factors such as decreased optical resolution and increased averaging in the direction parallel to the optical axis (which are both associated with the lower numerical apertures of lower-powered objectives). Alternatively, better resolution can also be obtained simply by increasing the magnitude of N, as shown in Fig. 10 *b*. In partitioning our full muscle images into quarter images, the value of N drops from 512 to 128, which, on the basis of Fig. 10 *b*, would not yield sufficient sarcomere length resolution (i.e., at a sarcomere length of 2.5 μm, the resolution is only 0.1 μm). We have overcome this problem by zero padding the data to the original N value of 512. Alternative methods such as the chirp-Z transform can also be employed to increase the sarcomere length resolution and may in fact be more efficient than zero padding (cf. Roose et al., 1993). It should be noted that in using the centroid frequency we are increasing our resolution by not restricting the sarcomere length assessment to discrete frequencies. Although significant increases in spatial resolution could be achieved through the use of linear (i.e., one-dimensional) charge coupled device arrays or line-

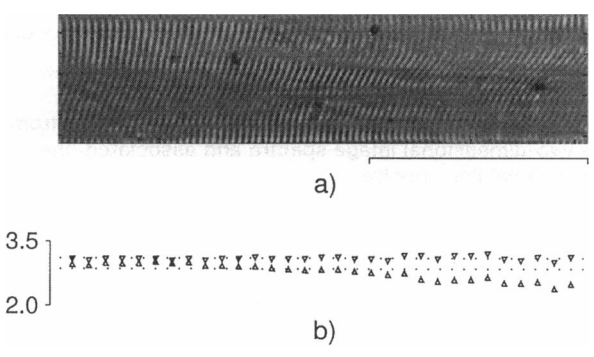

FIGURE 9 (*a*) Image of a fiber segment exhibiting skewed striations. (*b*) Sarcomere length distributions obtained using short time spectral estimation (*inverted triangles*, one-dimensional analysis; *upright triangles*, two-dimensional analysis). The top and bottom dotted lines represent the mean sarcomere lengths as estimated by examining the full line and image spectra, respectively.

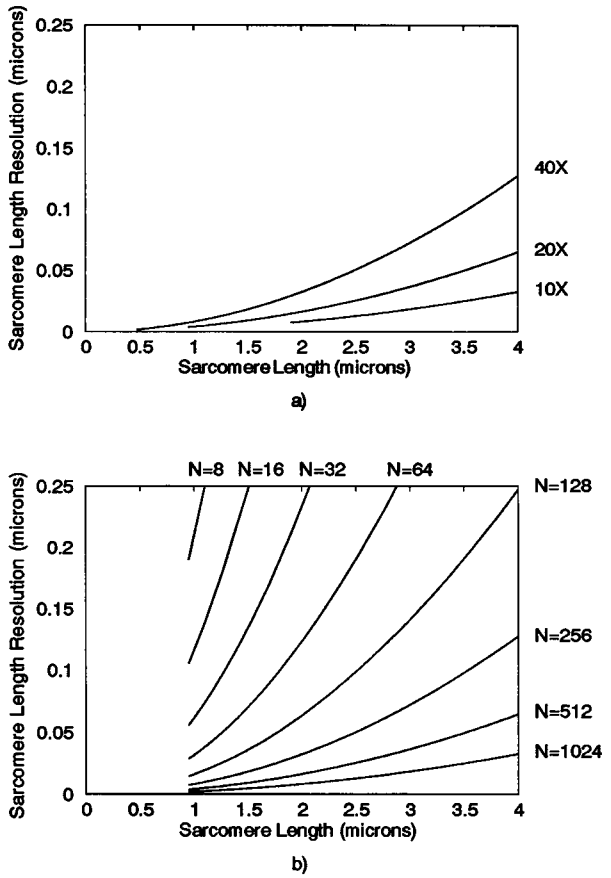

FIGURE 10 (*a*) Sarcomere length resolution as a function of sarcomere length and image resolution for the specific case in which $N = 512$. (*b*) Sarcomere length resolution as a function of sarcomere length and N for the specific case in which $\Delta l = 0.475$ μm, corresponding to 200× magnification.

scan cameras, such resolution comes at the expense of losing the two-dimensional image information. In addition, in using such devices care must be taken to align the sensor axis with the fiber axis to minimize errors that result from misalignment (Roos et al., 1982).

In terms of temporal resolution, there are two main issues to be considered: the acquisition rate and the analysis rate. In terms of the former, we are limited by the 60-Hz field rate/30-Hz frame rate of the RS-170 video standard (cf. Inoue, 1986). Roos and Parker (1990) addressed this issue by modifying a standard video camera in such a manner that only the top quarters of the image fields are scanned, effectively increasing the imaging rate to 240 Hz. Even greater increases in the imaging rate could be achieved by further reducing the vertical resolution of the image fields. The analysis rate, on the other hand, is generally significantly slower because of the computational load associated with calculating two-dimensional Fourier transforms. Specifically, with a 66-MHz 80486-based IBM compatible computer the time required to compute a 128×512 Fourier transform is of the order of 3 s. Hence, using our existing setup, the analysis must be performed off-line by analyzing the images recorded with the S-VHS video recorder.

There are a number of ways in which the computation time can be scaled down. Gannier et al. (1993) employ a method in which they reduce the two-dimensional images into one-dimensional line luminances (by simply summing the images across their columns) and then calculating the associated one-dimensional Fourier transforms. However, striation skewness can significantly influence the luminance profiles derived by such analysis, which in turn would affect the sarcomere length measurements. Deskewing procedures have been proposed (e.g., Periasamay et al., 1990), but it may be difficult to extend these procedures to situations in which multiple skew planes have developed. Alternatively, there are other means by which the two-dimensional analysis method can be optimized. First, the software can be optimized by writing the program in assembly language (Gannier et al., 1993). Second, the calculation can be implemented in hardware through the use of digital signal processors. Finally, we may be able to employ other, more efficient orthogonal transforms to obtain the spectra. Examples of these are the Walsh and Haar functions that have been employed in numerous applications such as filtering, image enhancement, and pattern recognition (cf. Beauchamp, 1984). The Haar transform is of particular interest because, unlike the Fourier transform, it includes both global and local basis functions and could potentially be used directly to assess local sarcomere heterogeneity. Table 5 compares the computation times for the Fourier, Walsh, and Haar transforms and shows the dramatic computational savings that can be achieved by employing these various transforms. Further decreases in computation time can be achieved by implementing the transforms in hardware (Smith, 1980). In a preliminary analysis of the utility of these functions in assessing sarcomere length, we found good correspondence between the Fourier and Walsh spectra, whereas the Haar spectra tended to be more complicated (Slawnych et al., 1994).

TABLE 5 Relative comparison of Fourier, Walsh, and Haar transforms

Transform	Relative Time	Data Storage (kB)
Fourier	32.69	4
Walsh	5.52	3
Haar	1.00	4

It should be stated that there currently exists an alternative class of image-analysis-based methods that offer significantly better temporal resolution than the method presented here. These methods are based on a phase-locked loop technique in which the output of a voltage-controlled oscillator is phase locked to the video signal (Claes et al., 1980; deClerck et al., 1980; Myers et al., 1982; Krueger and Denton, 1992). Inasmuch as the frequency of the voltage-controlled oscillator is matched to the frequency of the video signal, FM demodulation of the former yields a voltage directly proportional to the instantaneous frequency of the video signal. Early implementations of this approach were based on the analysis of standard 60-Hz video signals (Claes et al., 1980; deClerck et al., 1981), but the use of photodiode arrays has increased the temporal resolution up to 500 Hz (Myers et al., 1982; Krueger and Denton, 1992). The recent implementation by Krueger and Denton (1992) is particularly interesting inasmuch as it allows for the simultaneous assessment of sarcomere length in two different regions of the fiber. However, although the phase-locked loop approach offers many advantages, it is a one-dimensional-based approach and hence cannot detect striation skewness.

The temporal resolution of image-analysis-based methods is significantly lower than that achievable with laser-diffraction-based methods, but there is a method by which both high temporal resolution and localization can be achieved. Specifically, laser-diffraction- and image-analysis-based methods can be used in tandem (Horowitz et al., 1992).

At short sarcomere lengths (<2.4 μm), contractions were generally associated with some degree of sarcomeric redistribution, which effectively reduced the contrast between the I and A bands. In an effort to improve the contrast, we evaluated several image enhancement techniques such as bandpass, Wiener, and homomorphic filtering. We found that although these methods improved the contrast of the images, they did not significantly change the sarcomere length measurements and hence did not warrant the additional computational expense. It should be noted that improved contrast can be obtained without computational penalty by optimizing the optical system. Two examples of such optimization are polarization microscopy (Periasamy et al., 1990) and Hoffman demodulation contrast microscopy (Krueger and Denton, 1992).

As we showed in Fig. 9, better estimates of local sarcomere length can be obtained by dividing the full image

into multiple subimages spanning only a small fraction of the full image. However, it should be noted that this increased "localization" comes at the cost of a greatly increased computational load. In addition, there is a practical limit as to the minimum subimage size that can be employed beyond which the frequency response deteriorates significantly.

To summarize, we have shown that Fourier-based analysis of full and partial muscle images is well suited to the analysis of local sarcomere heterogeneity in skeletal muscle fiber segments. A typical application of this method would be assessing protocols for minimizing sarcomere heterogeneity during contraction. Examples of such protocols include Brenner cycling (Brenner, 1983) and presoaking the fiber segment in "rinse" solutions in which the Ca^{2+} buffering capacity has been greatly reduced (Moisescu and Thieleczek, 1978; Ford et al., 1991; Moss et al., 1991). This method would also be well suited to the analysis of single cardiac cell dynamics. Specifically, these cells are short enough that all the sarcomeres can be visualized in the field of view. In addition, their short sarcomere lengths facilitate good sarcomere length resolution, as shown in Fig. 10.

This research was supported by the Medical Research Council of Canada.

REFERENCES

Anazawa, T., K. Yasuda, and S. Ishiwata. 1992. Spontaneous oscillation of tension and sarcomere length in skeletal myofibrils. Microscopic measurement and analysis. *Biophys. J.* 61:1099–1108.

Beauchamp, K. G. 1984. Applications of Walsh and Related Functions with an Introduction to Sequency Theory. Academic Press, Lancaster, England.

Brenner, B. 1983. Technique for stabilizing the striation pattern in maximally activated skinned rabbit psoas fibers. *Biophys. J.* 41:99–102.

Brenner, B. 1985. Sarcomeric domain organization within single skinned rabbit psoas muscle fibers and its effects on laser light diffraction patterns. *Biophys. J.* 48:967–982.

Claes, V. A., N. M. deClerck, E. R. VanOcken, and D. L. Brutsaert. 1980. New method for sarcomere measurements. *Fed. Proc.* 39:1729.

Cooley, J. W., and J. W. Tukey. 1965. An algorithm for the machine computation of simplex Fourier series. *Math. Comput.* 19:297–301.

deClerck, N. M., V. A. Claes, and D. L. Brutsaert. 1984. Uniform sarcomere behavior during twitch of intact single muscle fibers. *J. Mol. Cell Cardiol.* 16:735–745.

deClerck, N. M., V. A. Claes, E. R. VanOcken, and D. L. Brutsaert. 1981. Sarcomere distribution patterns in single cardiac cells. *Biophys. J.* 35: 237–242.

Ford, L. E., K. Nakagawa, J. Desper, and C. Y. Seow. 1991. Effect of osmotic compression on the force-velocity properties of glycerinated rabbit skeletal muscle cells. *J. Gen. Physiol.* 97:73–88.

Gannier, F., J. C. Bernengo, V. Jacquemond, and D. Garnier. 1993. Measurements of sarcomere dynamics simultaneously with auxotonic force in isolated cardiac cells. *IEEE Trans. Biomed. Eng.* 40:1226–1232.

Goldman, Y. E., and R. M. Simmons. 1979. A diffraction system for measuring muscle sarcomere length. *J. Physiol.* 292:5P–6P.

Goldman, Y. E., and R. M. Simmons. 1984. Control of sarcomere length in skinned muscle fibres of rana temporaria during mechanical transients. *J. Physiol.* 350:497–518.

Goldspink, G., R. E. Larson, and R. E. Davies. 1970. Fluctuations in sarcomere length in the chick anterior and posterior latissmus dorsi muscles during isometric contraction. *Experientia.* 26:16–18.

Horowitz, A., H. P. M. Wussling, and G. H. Pollack. 1992. Effect of small release on force during sarcomere-isometric tetani in frog muscle fibers. *Biophys. J.* 63:3–17.

Huxley, A. F. 1980. Reflections on Muscle. Liverpool University Press, Liverpool, U.K.

Huxley, A. F., and L. D. Peachey. 1961. The maximum length for contraction in vertebrate striated muscle. *J. Physiol.* 156:150–165.

Inoue, S. 1986. Video Microscopy. Plenum Press, New York.

Judy, M. M., V. Summerour, T. LeConey, R. L. Roa, and G. H. Templeton. 1982. Muscle diffraction theory. Relationship between diffraction subpeaks and discrete sarcomere length distributions. *Biophys. J.* 37: 475–487.

Julian, F. J., M. R. Sollins, and R. L. Moss. 1978. Sarcomere length non-uniformity in relation to tetanic responses of stretched skeletal muscle fibres. *Proc. R. Soc. London Ser. B.* 200:109–116.

Kawai, M., and I. D. Kuntz. 1973. Optical diffraction studies of muscle fibers. *Biophys. J.* 13:857–876.

Krueger, J. W., D. Forletti, and B. A. Wittenberg. 1980. Uniform sarcomere shortening behavior in isolated cardiac muscle cells. *J. Gen. Physiol.* 76:587–607.

Krueger, J. W. 1988. Measurement and interpretation of contraction in isolated cardiac cells. *In* Biology of Isolated Adult Cardiac Myocytes. W. A. Clark, R. S. Decker, and T. K. Borg, editors. 172–186.

Krueger, J. W., and A. Denton. 1992. High resolution measurement of striation patterns and sarcomere motions in cardiac muscle cells. *Biophys. J.* 61:129–144.

Leung, A. F. 1982. Calculation of the laser diffraction intensity of striated muscle by numerical methods. *Comput. Programs Biomed.* 15:169–174.

Leung, A. F. 1984. Fine structures in the light diffraction pattern of striated muscle. *J. Musc. Res. Cell Motil.* 5:535–558.

Lieber, R. L., K. P. Roos, B. A. Lubell, C. W. Cline, and R. J. Baskin. 1983. High-speed digital data acquisition of sarcomere length from isolated skeletal and cardiac muscle cells. *IEEE Trans. Biomed. Eng.* 30:50–57.

Lieber, R. L., Y. Yeh, and R. J. Baskin. 1984. Sarcomere length determination using laser diffraction. *Biophys. J.* 45:1007–1016.

Morgan, D. L. 1990a. New insights into the behavior of muscle during active lengthening. *Biophys. J.* 57:209–221.

Morgan, D. L. 1990b. Modeling of lengthening muscle: the role of intersarcomere dynamics. *In* Multiple Muscle Systems: Biomechanics and Movement Organization. J. M. Winters and S. L.-Y. Woo, editors. Springer-Verlag, New York. 46–56.

Moisescu, D. G., and R. Thieleczek. 1978. Calcium and strontium concentration changes within skinned muscle preparations following a change in the external bathing solution. *J. Physiol.* 275:241–262.

Moss, R. L., G. G. Giulian, and M. L. Greaser. 1983. Effects of EDTA treatment upon the protein subunit composition and mechanical properties of mammalian single skeletal muscle properties. *J. Cell. Biol.* 96:970–978.

Moss, R. L., L. O. Nwoye, and M. L. Greaser. 1991. Substitution of cardiac troponin C into rabbit muscle does not alter the length dependence of Ca^{2+} sensitivity of tension. *J. Physiol.* 440:273–289.

Myers, J. R., R. Tirosh, R. C. Jacobson, and G. H. Pollack. 1982. Phase lock loop measurement of sarcomere length with high time resolution. *IEEE Trans. Biomed. Eng.* 29:463–466.

Niggli, E. 1988. A laser diffraction system with improved sensitivity for long-time measurements of sarcomere dynamics in isolated cardiac myocytes. *Pflugers Arch.* 411:462–468.

Periasamy, A., D. H. Burns, D. N. Holdren, G. H. Pollack, and K. Trombitas. 1990. A-Band shortening in single fibers of frog skeletal muscle. *Biophys. J.* 57:815–828.

Roos, K. P. 1987. Sarcomere length uniformity determined from three-dimensional reconstruction of resting isolated heart cell striation patterns. *Biophys. J.* 52:317–327.

Roos, K. P., A. C. Bliton, B. A. Lubell, J. M. Parker, M. J. Patton, and S. R. Taylor. 1989. High speed striation pattern recognition in contracting cardiac myocytes. *Proc. Soc. Photo-opt. Instrum. Eng.* 1063:29–41.

Roos, K. P., and A. J. Brady. 1982. Individual sarcomere length determination from isolated cardiac cells using high-resolution optical microscopy and digital image processing. *Biophys. J.* 40:233–244.

Roos, K. P., A. J. Brady, and S. T. Tan. 1982. Direct measurement of sarcomere length from isolated cardiac cells. *Am. J. Physiol.* 242: H68–H78.

Roos, K. P., and A. F. Leung. 1987. Theoretical Fraunhofer light diffraction patterns calculated from three-dimensional sarcomere arrays imaged from isolated cardiac cells at rest. *Biophys. J.* 52:329–341.

Roos, K. P., and J. M. Parker. 1990. A low cost two-dimensional digital image acquisition sub-system for high speed microscopic motion detection. *Proc. Soc. Photo-opt. Instrum. Eng.* 1205:134–141.

Roos, K. P., and S. R. Taylor. 1988. High speed digital imaging of rat cardiac myocyte contractile dynamics. *In* Biology of Isolated Adult Cardiac Myocytes. W. A. Clark, R. S. Decker, and T. K. Borg, editors. Elsevier, New York. 398–401.

Roos, K. P., and S. R. Taylor. 1993. Video imaging and digital analysis of microscopic features in contracting striated muscle cells. *Opt. Eng.* 32:306–313.

Roose, S., B. Brichau, and E. W. Stijns. 1993. An efficient interpolation algorithm for Fourier and diffractive optics. *Opt. Commun.* 97: 312–318.

Rudel, R., and F. Zite-Ferenczy. 1979. Do laser diffraction studies on striated muscle indicate stepwise shortening? *Nature (London).* 278: 573–575.

Sidick, E., R. J. Baskin, Y. Yeh, and A. Knoesen. 1994. Rigorous analysis of light diffraction ellipsometry by striated muscle fibers. *Biophys. J.* 66:2051–2061.

Slawnych, M., L. Morishita, and B. H. Bressler. 1994. The utility of Walsh and Haar transforms in the analysis of muscle images. *Biophys. J.* 66(2):A277.

Smith, E. G. 1980. CAD design of a modularized fast Walsh–Hadamard transformation device. *ICCC 80, IEEE International Conference on Circuits and Computers.* 916–920.

Sundell, C. L., Y. E. Goldman, and L. D. Peachey. 1986. Fine structure in near-field and far-field laser diffraction patterns from skeletal muscle fibers. *Biophys. J.* 49:521–530.

Thornhill, R. A., N. Thomas, and N. Berovic. 1991. Optical diffraction by well-ordered muscle fibers. *Eur. Biophys. J.* 20:87–99.

Yeh, Y., R. J. Baskin, R. L. Lieber, and K. P. Roos. Theory of light diffraction by single muscle fibers. *Biophys. J.* 29:509–522, 1980.

Zite-Ferenczy, F., K. D. Haberle, R. Rudel, and W. Wilke. 1986. Correlation between the light diffraction pattern and the structure of a muscle fibre realized with Ewald's construction. *J. Musc. Res. Cell Motil.* 7:197–214.